Journal of the Korean Geo-Environmental Society
17(12): 65~72. (December, 2016) http://www.kges.or.kr
ISSN 1598-0820
DOI https://doi.org/10.14481/jkges.2016.17.12.65

# Stress Distribution of Buried Concrete Pipe Under Various Environmental Conditions

Janggeun Lee[1] · Jae Mo Kang[1] · Hoki Ban† · Changyeul Moon[2]

Received: October 4th, 2016; Revised: October 14th, 2016; Accepted: November 23rd, 2016

**ABSTRACT :** There are numerous factors that affect stress distribution in a buried pipe, such as the shape, size, and stiffness of the pipe, its burial depth, and the stiffness of the surrounding soil. In addition, the pipe can benefit from the soil arching effect to some extent, through which the overburden and surcharge pressure at the crown can be carried by the adjacent soil. As a result, the buried pipe needs to support only a portion of the load that is not transferred to the adjacent soil. This paper presents numerical efforts to investigate the stress distribution in the buried concrete pipe under various environmental conditions. To that end, a nonlinear elasto-plastic model for backfill materials was implemented into finite element software by a user-defined subroutine (user material, or UMAT) to more precisely analyze the soil behavior surrounding a buried concrete pipe subjected to surface loading. In addition, three different backfill materials with a native soil were selected to examine the material-specific stress distribution in pipe. The environmental conditions considering in this study the loading effect and void effects were investigated using finite element method. The simulation results provide information on how the pressures are redistributed, and how the buried concrete pipe behaves under various environmental conditions.

**Keywords :** Buried concrete pipe, Stress distribution in pipe, Hoop stress, Trust

## 1. Introduction

Pipelines are very important infrastructures that provide transportation of various substances vital to our everyday life. So, pipelines are often considered as our life line. Pipelines either above-ground or underground (buried) can be categorized into different types. Examples include water, sewer, gas, oil, electricity, and communication pipelines, as well as offshore pipelines, inland pipelines, in-plant pipelines, cross-mountain pipelines, and others.

The presence of buried pipes inevitably alters the state of geostatic stress in the ground. The degree of alteration varies with numerous factors such as the shape, size, and stiffness of the pipe, its burial depth, and the stiffness of the surrounding soil. As stated, in order to investigate stress distribution in pipe, the investigation of the soil pressure distribution is considered to be a necessary for the proper design and analysis procedures of a buried concrete pipe.

Although several researchers (Pettibone & Howard, 1976; Potter, 1985; Shumulevich et al., 1985; Sargand & Hazen, 1998; McGrath, 1998) have conducted laboratory and full-scale field tests to investigate soil pressure distribution around a buried pipe, most experimental efforts have focused on backfill materials. Soil pressure distribution is affected not only by the backfill materials, but also other environmental conditions, such as the loading type, the presence of a groundwater table, and voids formed around the buried pipe. These environmental conditions have not been fully considered in the procedure of pipeline analysis.

The performance of flexible pipes with nonuniform soil support was studied by Zarghamee (1986). The initial stress state and deformed configuration of a buried flexible pipe with nonuniform soil support were calculated by modeling the buried pipe as a cylindrical shell embedded in an elastic foundation. It was proved that a buried flexible pipe without an adequate haunch support will experience higher flexural strains at the invert of the pipe even in the absence of internal pressure.

Rajani et al. (1996) presented an analytical analysis of pipe-soil interaction for jointed water mains which consisted of cast or ductile iron and PVC pipes. They assumed that the pipes responded elastically to external/internal pressures

1) Geotechnical Division, Korea Institute of Construction Technology
† Department of Civil Engineering, Kangwon National University (Corresponding Author : hban@kangwon.ac.kr)
2) Department of Civil Engineering, Kangwon National University

as well as temperature changes. Variables affecting water main breaks were temperature, axial pipe-soil reaction modulus, pipe size, and type. The sensitivity analysis was conducted to identify key variables that played a major role in the overall behavior of buried water mains.

In addition, Zarghamee et al. (2002) conducted nonlinear finite element analyses using ABAQUS to predict the performance of prestressed concrete pipe with broken wires in a pipeline. The concrete model is a continuum plasticity-based, damage model based on two failure mechanisms of tensile cracking and compressive crushing. The crack patterns, crack width, pipe deflection, stress change in the wires, and concrete crushing as a function of presstress loss length were investigated. However, this study focused only on the performance of the pipe without considering soil-pipe interaction.

This paper presents the stress distributions in a buried concrete pipe obtained by performing intensive numerical simulations through the implementation of a nonlinear elasto-plastic model for backfill materials. With the developed soil model, more accurate soil pressure distributions around buried concrete could help assess hoop stress and circumferential thrust in pipe.

## 2. Finite element modeling

Three-dimensional finite element modeling was conducted using a software, ABAQUS. In the modeling, shell elements for buried concrete and solid elements for surrounding soils were used.

### 2.1 Constitutive models

A nonlinear elasto-plastic model was adopted for backfill materials to more accurately predict the response of surrounding soils in various loading conditions. For the nonlinear elastic part, the hyperbolic stress-strain relationship proposed by Duncan & Chang (1970) was employed. During the application of each load increment, the material is considered to be linearly elastic. However, different tangential elastic moduli are used according to the change of stresses at each incremental load. The tangential modulus ($E_t$) is defined as:

$$E_t = E_i\left[1-\frac{R_f(1-\sin\phi)(\sigma_1-\sigma_3)}{2c\cos\phi+2\sigma_3\sin\phi}\right]^2 \quad (1)$$

where $R_f$ = failure ratio

$E_i$ = initial modulus = $KP_a\left(\frac{\sigma_3}{P_a}\right)^n$

$P_a$ = atmosphere pressure (101.3 kPa)

$K$, $n$ = mateiral constants

c = cohesion

$\phi$ = friction angle

$\sigma_1$ and $\sigma_3$ = major and minor principal stress, respectively.

For the plastic part, the Drucker-Prager yield criterion with non-associated flow rule was employed. The Drucker-Prager yield criterion can be expressed in terms of deviatoric stress and hydrostatic stress as follows:

$$f(s,p)=\|s\|+\sqrt{2}(3\alpha p-k) \quad (2)$$

where s and p are the deviatoric and hydrostatic pressure, respectively; $\|s\|$ is the norm of deviatoric stress; $\alpha$ and $k$ are material constants.

A non-associated flow rule is then considered by choosing the plastic potential,

$$g(\sigma)=\|s\| \quad (3)$$

which gives the plastic strain rate, $\dot{\varepsilon}^p$, in the following form;

$\dot{\varepsilon}^p = \dot{\lambda}\frac{\partial g}{\partial \sigma} = \dot{\lambda}\mathbf{n}$ for loading

$\dot{\varepsilon}^p = 0$ otherwise

in which $\mathbf{n}=\frac{s}{\|s\|}$ and $\dot{\lambda}$ is the plastic strain parameter.

The aforementioned nonlinear elasto-plastic model was implemented into ABAQUS via user-defined material subroutine called UMAT.

The buried concrete pipe was characterized as a linearly elastic plastic material. A damage model is incorporated in the plastic component, in which the behavior of reinforcement is modeled by considering the tension stiffening effect.

### 2.2 Model mesh and boundary conditions

Fig. 1 presents the finite element mesh for the simulations.

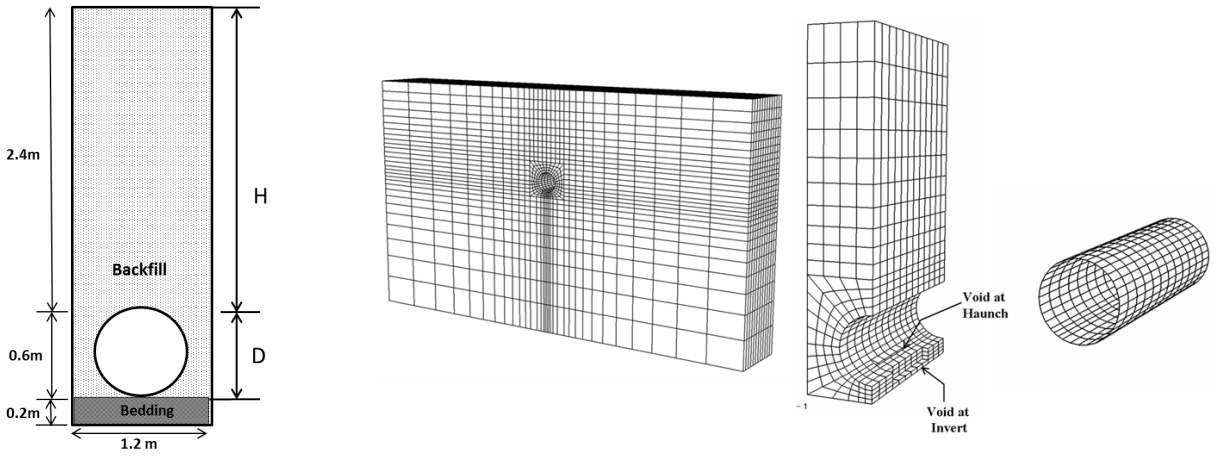


Fig. 1. Schematic drawing and finite element mesh for simulation

As mentioned earlier, the concrete pipe was modeled using a four-node, quadrilateral, and stress/displacement shell element with reduced integration (S4R in ABAQUS). The surrounding soils are modeled by linear displacement with reduced integration continuum element (C3D8R in ABAQUS).

As illustrated in Fig. 1, the finite element mesh extends to a depth of seven times the pipe diameter below the invert, and laterally to ten times the diameter away from the springline. This boundary has been shown to be sufficient to eliminate the boundary effect. This implies that changes of stress and displacement on the wall boundaries are negligible.

## 2.3 Material properties used for the simulations

The properties of concrete pipe used for shell elements include compressive and tensile softening. The stress-strain relationship of concrete employed in this simulation is presented in Fig. 2. The curve in compression is from Todeshini et al. (1964) and the curve in tension is from Zarghamee and Fok (1990).

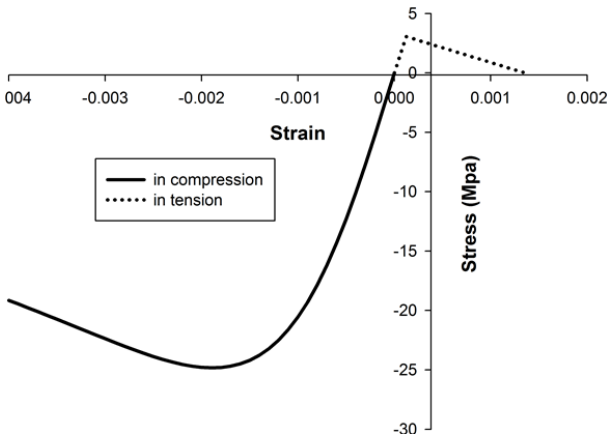


Fig. 2. Stress-strain relationship buried concrete pipe used in this study

The material properties of surrounding soils and concrete pipe used in the simulations were obtained from published literature (McGrach, 1998; Selig, 1990; Zarghamee & Fok, 1990; Zharghamee et al., 2002) and ASTM C 76, and are presented in Tables 1 and 2, respectively. In Table 1, SW, ML, and CL are well-graded sand, low-plastic silt, and low to medium-plastic silty clay, respectively. The values of 80, 95, and 100 are the maximum dry densities according to ASSHTO T-99 used in the standard Proctor test.

In Table 2, f'c is the specified compressive strength of concrete, and f't is the tensile strength of concrete.

The analyses contain three steps, which involve determining

Table 1. Surrounding soil properties

| Material properties | Native soil | Backfill material | | |
|---|---|---|---|---|
| | Clay | SW95 | ML95 | CL95 |
| E (MPa) | 7 | - | - | - |
| v | 0.4 | 0.32 | 0.3 | 0.29 |
| $\gamma$ (kN/m$^3$) | 14 | 20.5 | 17.2 | 15.4 |
| K | - | 950 | 440 | 120 |
| n | - | 0.6 | 0.4 | 0.45 |
| $R_f$ | - | 0.7 | 0.85 | 0.86 |
| c (kN/m$^2$) | 30 | 0 | 28 | 48 |
| $\phi$ (deg) | 18 | 48 | 34 | 15 |

Table 2. Size and material properties of concrete pipe

| Internal diameter (mm) | Wall thickness (mm) | E (MPa) | v | f'c (MPa) | f't (MPa) |
|---|---|---|---|---|---|
| 609 | 76 | 24000 | 0.2 | 27.6 | 3.1 |

the initial stress conditions, the geostatic state, and the loading step. Since the behavior of soil depends on the current stress and strain fields, determining the initial conditions is the first step, in which the initial stress of the soil is defined. The initial vertical stress is assumed to vary linearly with depth, and the initial horizontal stress is determined by multiplying the initial vertical stress by the coefficient of earth pressure at rest. The geostatic step verifies whether the initial geostatic stress field predefined in the first step is in equilibrium with the applied loads and boundary conditions. The analysis cannot commence if the equilibrium is not achieved. a gravity load of 9.8 m/s$^2$ is applied to both the soil and pipe. After establishing the initial stress with appropriate boundary conditions, the loading step is then carried out.

## 3. Simulation results

### 3.1 Surface loading effect

The internal and external hoop stress distributions along the pipe circumference under different loading conditions with gravelly sand, silty sand, and silty clay backfill all in a clay native soil are presented in Fig. 3. Each figure includes three sets of curves for three different loading conditions of longitudinal, transverse and uniform loading. For each loading condition, there are two curves, one for intrados and the other for extrados. Also included in the figures is a dot-dashed horizontal line showing the maximum tensile stress of the concrete pipe. As shown, the distribution is somewhat symmetric about the springline with the magnitude at the crown a little higher than that at the invert. The general trend shows maximum stresses at springline and minimum stresses at shoulder and haunch areas. In terms of absolute value, the hoop stresses at shoulder and haunch are equal on intrados and extrados. The stresses at crown are significantly larger than that at invert when the trench is filled with gravelly sand and silty sand. However, such a stress difference between crown and invert is not as obvious for silty clay trench material.

As would be expected, tensile hoop stress occurs on extrados at springline and on intrados at crown and invert. As seen, the magnitude of hoop stress is largest under uniform loading followed by longitudinal then transverse loading. It

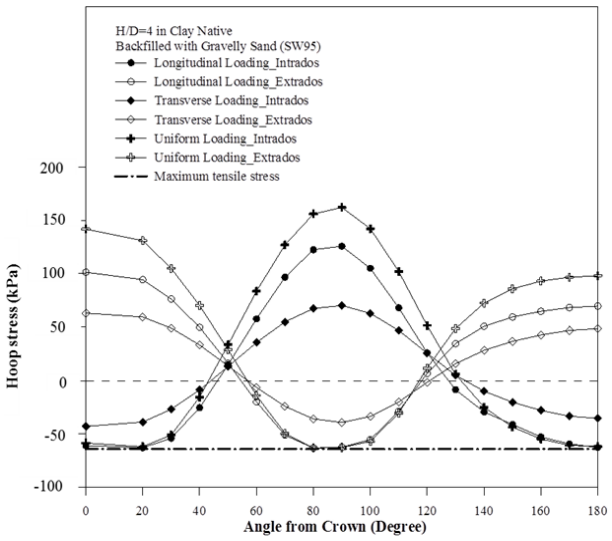


(a)

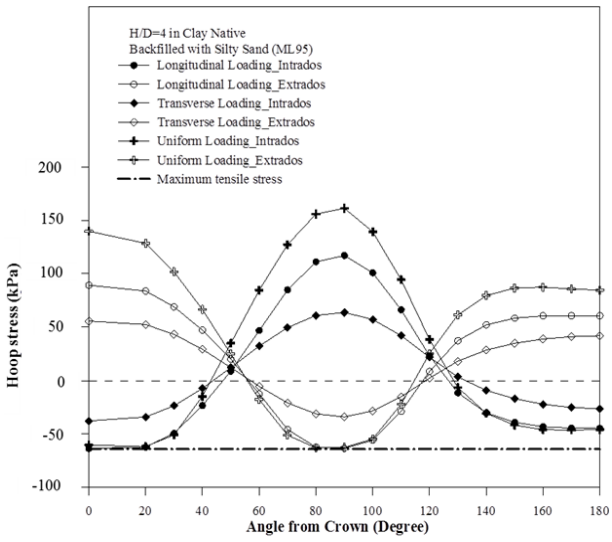


(b)

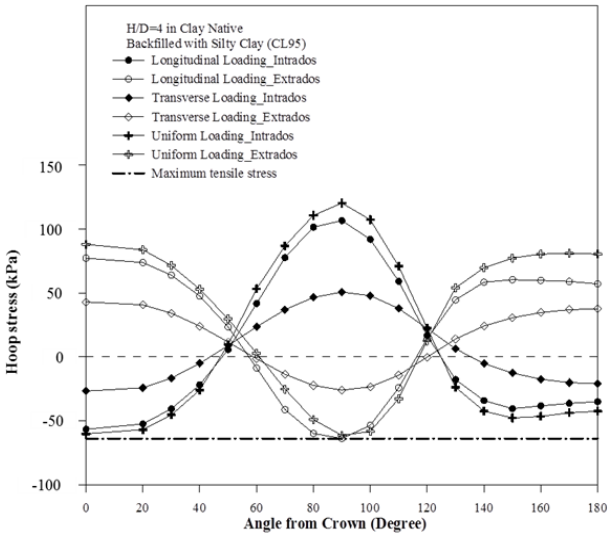


(c)

Fig. 3. Variation of hoop stress along pipe circumference under longitudinal, transverse, and uniform loading; (a) SW95; (b) ML95; and (c) CL95

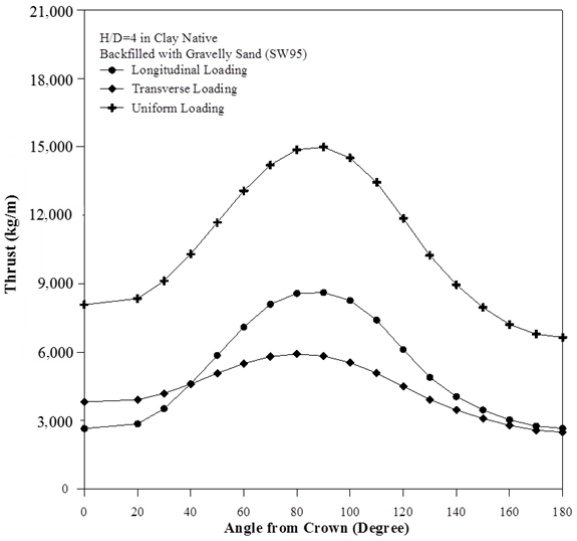


(a)

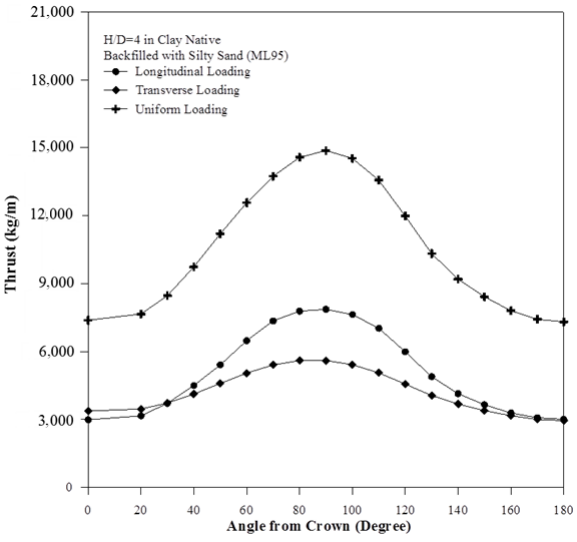


(b)

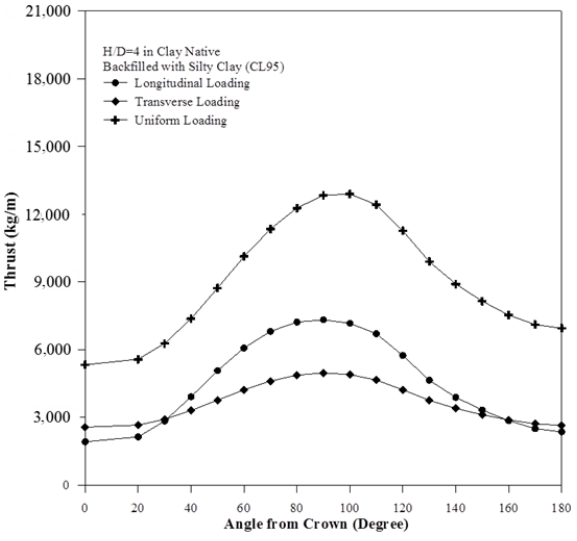


(c)

Fig. 4. Variation of circumferential thrust under longitudinal, transverse, and uniform loading; (a) SW95; (b) ML95; and (c) CL95

is noted that the compressive hoop stress of uniform loading condition is larger than the other two loading conditions; however, the tensile hoop stress of uniform loading at crown and springline is less than longitudinal loading. This is because under uniform surface loading of 8.6 KPa the hoop stress exceeds maximum tensile strength and undergoes tensile stiffening resulting in the decease of hoop stress.

The circumferential thrust distributions in the pipe under different loading conditions are presented in Fig. 4 (a) for gravelly sand backfill, Fig. 4 (b) for silty sand backfill, and Fig. 4 (b) for silty clay backfill. As would be expected, the maximum circumferential thrust occurs at the springline for all conditions, irrespective of types of loading and backfill materials.

As shown in Fig. 4 (a), the maximum circumferential thrust among three different loading conditions occurs when the pipe is subjected to the uniform loading. It is noticed that under transverse loading the circumferential thrust between crown and shoulder is higher than that of longitudinal loading. Around the springline, the longitudinal loading induces considerably greater hoop stress than the transverse loading. Below the lower haunch, the hoop stresses induced by the two loadings are very close to each other.

For silty sand presented in Fig. 4 (b), and silty clay in Fig. 4 (c), the pattern of circumferential thrust distribution resembles that of gravelly sand. However, the figures reveal that the intensity of thrust is considerably smaller under transverse loading than the other two loading conditions.

## 3.2 Void effect

The effect of a void at invert on hoop stress distributions in pipe wall under longitudinal loading is shown in Fig. 5 (a) for gravelly sand backfill, Fig. 5 (b) for silty sand backfill, and Fig. 5 (c) for silty clay backfill. Each figure contains two sets of curves; one set for no-void and the other set for a void at invert. Also, there are two curves for each set – one curve for hoop stress on intrados and the other for extrados. Plus included in the figures is a dot-dashed horizontal line representing the maximum tensile stress of the concrete pipe. As illustrated in all of these three figures, the presence of a void at invert reduces the hoop stress in the pipe at invert as would be expected. Furthermore, there is no apparent influence on the hoop

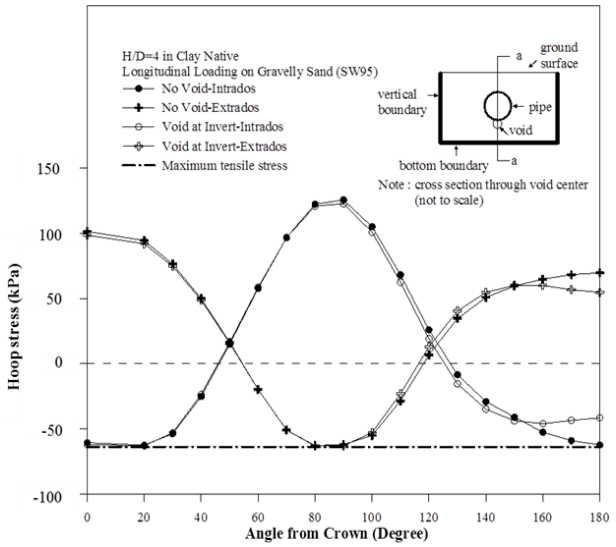


(a)

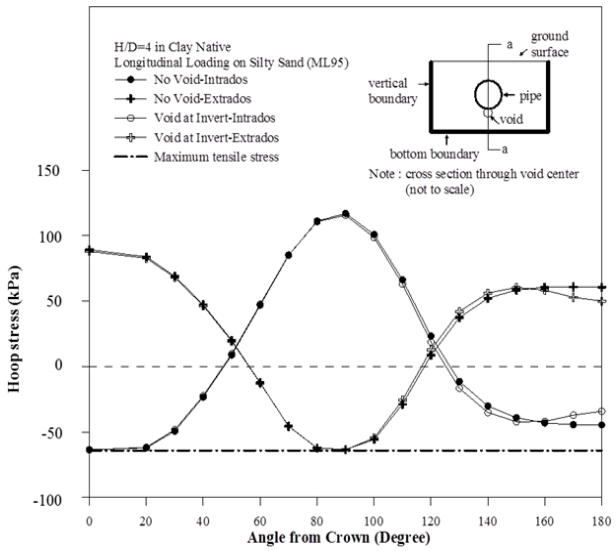


(b)

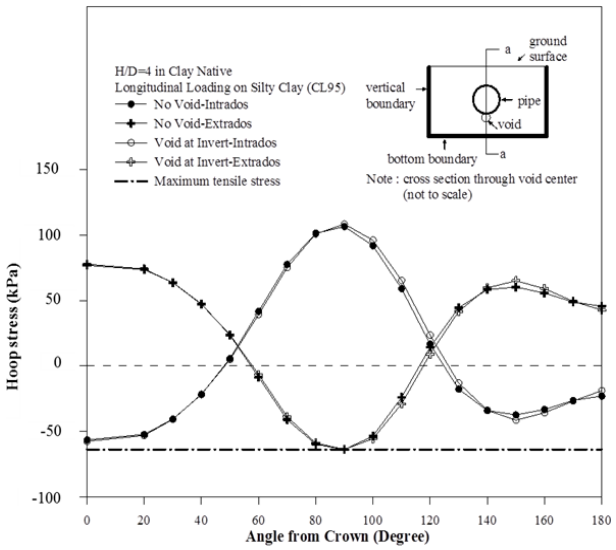


(c)

Fig. 5. Comparison of hoop stress between no-void and with a void at invert; (a) SW95; (b) ML95; and (c) CL95

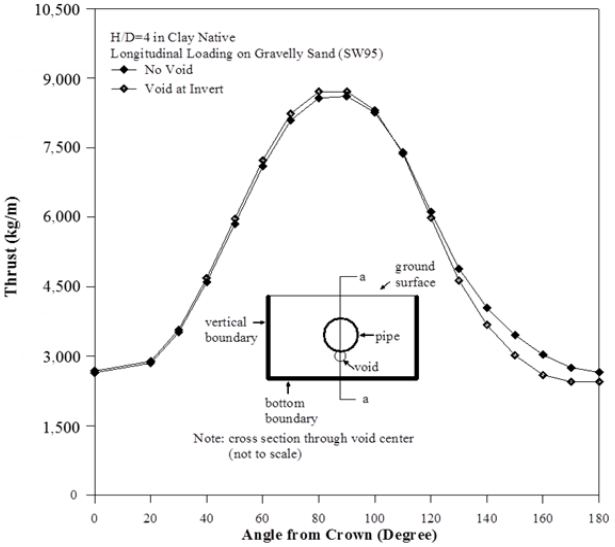


(a)

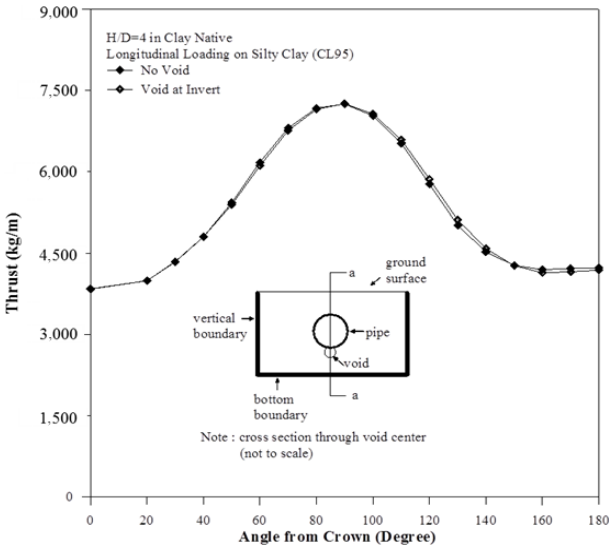


(b)

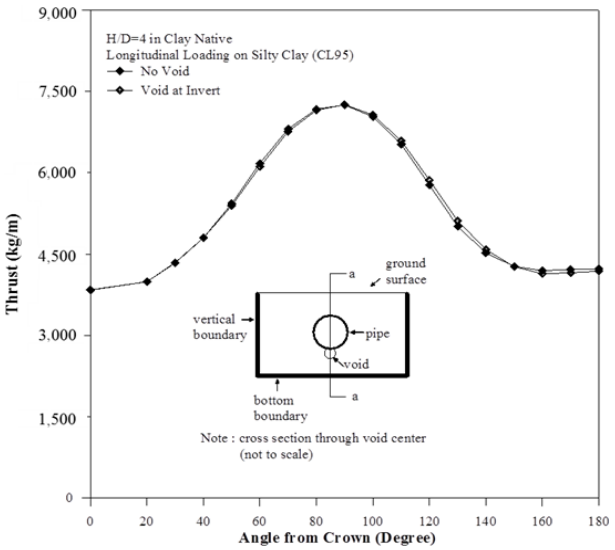


(c)

Fig. 6. Comparison of circumferential thrust between no-void and with a void at invert; (a) SW95; (b) ML95; and (c) CL95

stress at both crown and springline. Because of the void at invert, the reduced hoop stress at invert transfers to the haunch area resulting in the larger hoop stress around haunch as illustrated in these figures. The degree of influence of a void at invert depends on the backfill materials. Among three different backfill materials, the reduction of hoop stress at invert is the largest with gravelly sand backfill material, followed by silty sand and then silty clay. It can be explained that the relative stiffness between backfill material and void results in a larger reduction of hoop stress at invert.

As illustrated in Fig. 5 (a) for gravelly sand backfill material, the hoop stresses from crown to springline essentially are not affected by a void at invert. However, with a void at invert the hoop stresses at invert are smaller than those for no-void conditions. The void at invert also results in a decrease in hoop stress from springline to haunch and an increase in hoop stress in the lower haunch area. For silty sand and silty clay shown in Figs. 5 (b) and (d), the pattern of hoop stress distribution is similar to that for gravelly sand. However, the hoop stress at invert is greatly smaller than that for gravelly sand.

A comparison of circumferential thrust in the pipe wall between with and without a void at invert under the longitudinal loading is presented in Fig. 6 (a) for gravelly sand, Fig. 6 (b) for silty sand, and Fig. 6 (c) for silty clay. It is seen that the presence of void causes an increase in circumferential thrust from crown to springline, and that the circumferential thrust between springline and invert decreases due to the existence of void. However, the degree of influence of the void at invert varies with the type of backfill materials. The gravelly sand backfill material is affected most, followed by silty sand then silty clay.

## 4. Summary and Conclusions

This study investigated stress distribution in buried concrete pipe under various environmental conditions using finite element method. To do that, a nonlinear elasto-plastic soil model for backfill materials was implemented into commercial software through a user-defined subroutine. Intensive numerical simulations were conducted under various environmental conditions regarding loading types (longitudinal, transverse, or uniform) and the presence of void at invert. This study provides a better understanding of the load transfer mechanism to a buried concrete pipe, and the resulting stress distribution in pipe around the pipe, which can be used as a basis for the environment-related concrete pipe design process. Based on the simulation results, the following conclusions can be made:

(1) The hoop stress around pipe was strongly influenced by the loading type. The smallest and largest hoop stresses occur for transverse and uniform loading, respectively. It was also observed that the hoop stresses pressures under uniform and longitudinal loading nearly reached the maximum tensile stress that may start softening of the concrete pipe.
(2) The circumferential thrust distributions also showed similar trends to the hoop stress distribution under different loading conditions. It is noted that thrusts for silty sand and silty clay were considerably small under transverse loading condition.
(3) The presence of voids at the invert reduced the hoop stress at the invert only, and there was no distinct influence at both the crown and the springline. However, the reduced hoop stress around the invert area transferred to the haunch area, resulting in greater hoop stress around the haunch area.
(4) A void at invert induced a higher circumferential thrust at invert than that of no-void condition. the increased thrust transferred to the haunch zone of the concrete pipe, which is opposite result to the hoop stress distribution with a void at invert.

## Acknowledgement

This research was supported by a grant from the Strategic Research Project (Development of lifeline design and construction technology for rescuing lives from collapsed buildings), funded by the Korea Institute of Civil Engineering and Building Technology.

## References

1. Duncan, J. M. and Chang, C. Y. (1970), Nonlinear analysis of stress and strain in soils. Journal of Soil Mechanics and

Foundations Division, ASCE, Vol. 95, No. 5, pp. 1629~1653.
2. McGrath, T. J. (1998), Pipe-soil interactions during backfill placement, Ph.D. Thesis, University of Massachusetts, Amherst, MA.
3. Pettibone, C. H. and Howard, A. K (1976), Distribution of soil pressures on concrete pipe, Journal of Pipeline Division, ASCE, Vol. 93, No. 2, pp. 85~102.
4. Potter, J. C. (1985), Effects of vehicles on buried high pressure pipe, Journal of Transportation Engineering, Vol. 111, No. 3, pp. 224-235.
5. Rajani, B., Zhan, C. and Kuraoka, S. (1996), Pipe-soil interaction analysis of jointed water mains, Canadian Geotechnical Journal, Vol. 33, pp. 393~404.
6. Sargand, S. M. and Hazen, G. A. (1998), Field verification of standard installation direct method for concrete pipe, Ohio Research Institute for Transportation and the Environment.
7. Selig, E. T. (1990), Soil properties for plastic pipe installation, Buried Plastic Technology, STP1093, Philadelphia, Pa: pp. 141~158.
8. Shumulevich, I., Galili, N. and Foux, A. (1985), Soil stress distribution around buried pipes, Journal of Transportation Engineering, Vol. 112, No. 5, pp. 481~493.
9. Todeschini, C. E., Bianchini, A. C. and Kesler, C. E. (1964), Behavior of concrete columns reinforced with high strength steels, ACI Journal, Proceeding, Vol. 61, No. 5, pp. 710~716.
10. Zarghamee, M. S. (1986), Buried flexible pipe with nonuniform soil support, Journal of Transportation Engineering, ASCE, Vol. 112, No. 4, pp. 400~415.
11. Zarghamee, M. S. and Fok, K. L. (1990), Analysis of prestressed concrete pipe under combined loads, Journal of Structural Engineering, ASCE, Vol. 116, No. 7, pp. 2022~2039.
12. Zarghamee, M. S., Eggers, D. W. and Ojdrovic, R. P. (2002), Finite-element modeling of failure of PCCP with broken wires subjected to combined loads, Proceedings of 2002 pipelines, ASCE specialty conference, Cleveland, OH, 4-7 August 2002.